

PHYSICS

Direct imaging of electron transfer and its influence on superconducting pairing at FeSe/SrTiO₃ interfaceWeiwei Zhao,^{1,2*} Mingda Li,^{3,4,5*} Cui-Zu Chang,^{1,4,*†} Jue Jiang,¹ Lijun Wu,⁵ Chaoxing Liu,¹ Jagadeesh S. Moodera,^{4,6} Yimei Zhu,^{5†} Moses H. W. Chan^{1†}

The exact mechanism responsible for the significant enhancement of the superconducting transition temperature (T_c) of monolayer iron selenide (FeSe) films on SrTiO₃ (STO) over that of bulk FeSe is an open issue. We present the results of a coordinated study of electrical transport, low temperature electron energy-loss spectroscopy (EELS), and high-angle annular dark-field scanning transmission electron microscopy (HAADF-STEM) measurements on FeSe/STO films of different thicknesses. HAADF-STEM imaging together with EELS mapping across the FeSe/STO interface shows direct evidence of electrons transferred from STO to the FeSe layer. The transferred electrons were found to accumulate within the first two atomic layers of the FeSe films near the STO substrate. An additional Se layer is also resolved to reside between the FeSe film and the TiO₂-terminated STO substrate. Our transport results found that a positive backgate applied from STO is particularly effective in enhancing T_c of the films while minimally changing the carrier density. This increase in T_c is due to the positive backgate that “pulls” the transferred electrons in FeSe films closer to the interface and thus enhances their coupling to interfacial phonons and also the electron-electron interaction within FeSe films.

INTRODUCTION

Although bulk FeSe has a superconducting transition temperature T_c of 9.4 K (1, 2), a scanning tunneling microscopy (STM) study of 1-unit cell (UC) FeSe film on SrTiO₃ (STO) substrate in 2012 found a superconducting gap of 20 meV (3). Despite the ensuing intensive experimental (4–20) and theoretical studies (21–28), the exact mechanism responsible for the highly enhanced T_c in this system is still lacking. An angle-resolved photoemission spectroscopy (ARPES) experiment (7) found a replica band in a 1-UC FeSe film on STO attributable to the strong coupling between electrons in the FeSe layer and an optical phonon mode of the underlying STO. This is consistent with the proposal that the high T_c of the FeSe/STO system is due to the stronger pairing of the electrons in the FeSe film that is enabled by the STO phonons (21). A number of recent experiments investigated the effect of doping electrons into 3-UC and thicker FeSe films grown on different substrates (STO, MgO, or graphene) and also on free-standing FeSe flakes by depositing potassium (29, 30) or liquid-gating layers (31, 32) onto these films/flakes. Enhancements of T_c to near and above 40 K were found. Ex situ transport and Meissner effect measurements on 1-UC FeSe films found onset of superconductivity just above 40 K and zero resistance around 23.5 K (8). A recent STM study by Tang *et al.* (33) found that the deposition of potassium can induce superconducting gaps in 2-UC FeSe/STO films, which were previously not found by STM (3) and ARPES (10) techniques. On the other hand, the same STM study (33) also found that the superconductivity in 1-UC FeSe on STO is continuously suppressed with

increasing potassium coverage. Nevertheless, these electron-doping experiments on thicker films led to the suggestion that STO plays a role similar to potassium in enhancing the T_c of the 1-UC FeSe/STO system, namely, as an electron donor to the film. To validate STO as the electron donor responsible for the enhancement of T_c in FeSe films, it is crucial to have clear and direct evidence of charge transfer across the interface from STO to the FeSe film.

Here, we report a complementary Hall transport, atomically resolved electron energy-loss spectroscopy (EELS) and high-angle annular dark-field scanning transmission electron microscopy (HAADF-STEM) studies on the same 1-, 8-, and 14-UC FeSe films on STO. Transport measurements were also carried out in a number of other 1- and 2-UC films. The high spatial resolution (~0.02 nm) EELS mapping across the FeSe/STO interface at 10 K shows an explicit and unambiguous blue shift of energy, which is induced by the screening potential caused by electron charge transfer from STO to the FeSe films. According to the profile of screening potential, the transferred electrons accumulate within the first two FeSe UC near the interface, irrespective of the thickness of the FeSe film. Our systematic transport measurements confirm that the T_c of the 1-UC films can be enhanced by thermal annealing [which introduces electrons to the film (5, 9)] and also by backgating via STO with a positive potential (9). We found that backgating is particularly effective in enhancing the T_c without significantly changing the carrier density of the films. This lends support to the model of electron-phonon coupling across interface as a mechanism for high T_c (19, 21) because the positive potential tends to “pull” the interfacial electrons closer to the high Debye temperature STO phonon bath. We note that the electron-electron interaction within the FeSe film (34–36) should also be strengthened by gating in such an interfacial two-dimensional electron gas (2DEG) as compared to bulk carriers due to the lowering of its dimension (37).

RESULTS

Superconducting FeSe/STO films

The FeSe films were grown on heat-treated TiO₂-terminated insulating STO (001) substrates by molecular beam epitaxy (MBE) under a

¹Center for Nanoscale Science and Department of Physics, Pennsylvania State University, University Park, PA 16802–6300, USA. ²State Key Laboratory of Advanced Welding and Joining and Research Center of Flexible Printed Electronic Technology, Harbin Institute of Technology, Shenzhen 518055, People's Republic of China. ³Department of Nuclear Science and Engineering, Massachusetts Institute of Technology, Cambridge, MA 02139, USA. ⁴Francis Bitter Magnet Laboratory and Plasma Science and Fusion Center, Massachusetts Institute of Technology, Cambridge, MA 02139, USA. ⁵Condensed Matter Physics and Materials Science Department, Brookhaven National Laboratory, Upton, NY 11973, USA. ⁶Department of Physics, Massachusetts Institute of Technology, Cambridge, MA 02139, USA.

*These authors contributed equally to this work

†Corresponding author. Email: mhc2@psu.edu (M.H.W.C.); zhu@bnl.gov (Y.Z.); cxc955@psu.edu (C.Z.C.).

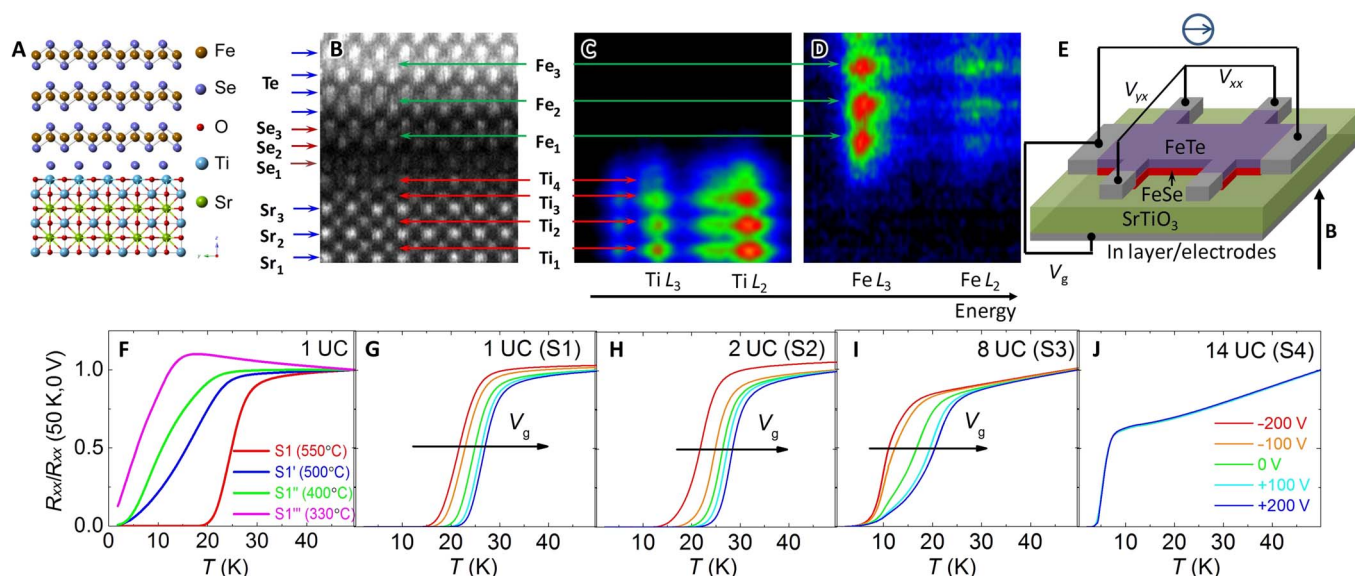


Fig. 1. Superconducting FeSe films on STO substrates. (A) Super cell of FeSe on top of STO (001), inferred from combined HAADF image and EELS data. (B) The HAADF-STEM image of the 1-UC FeSe film on STO with FeTe capping layers. (C and D) The integrated Ti $L_{3,2}$ and Fe $L_{3,2}$ EELS after subtracting background in false color with increasing intensity in the black-blue-green-red sequence. (E) Schematics of the gate-tuned six-terminal Hall bar device of FeSe films on STO with FeTe capping layer. For clarity, Te film on FeTe is not shown. (F) Normalized R_{xx} versus T for 1-UC films annealed at different temperatures for 2 hours post MBE growth: S1 (550°C), S1' (500°C), S1'' (400°C), and S1''' (330°C). (G to J) Normalized R_{xx} versus T at various backgating voltage V_g for the (G) S1 (1 UC), (H) S2 (2 UC), (I) S3 (8 UC), and (J) S4 (14 UC) films under the optimal annealing condition at 550°C.

pressure of 5×10^{-10} torr. Four 1-UC-thick FeSe films that annealed at 550°, 500°, 400°, and 330°C are labeled respectively as S1 (1 UC), S1' (1 UC), S1'' (1 UC), S1''' (1 UC). Figure 1F shows S1 (1 UC), annealed at 550°C has the highest T_c . Three thicker FeSe films of 2, 8, and 14 UC were also annealed at 550°C and are denoted as S2 (2 UC), S3 (8 UC), and S4 (14 UC). A 14-UC FeTe followed by 10-nm-thick Te film was deposited on all samples as capping layers (8) to prevent contamination for ex situ transport and EELS measurements. The cross-sectional high-resolution STEM and EELS measurements of the S1 (1 UC) film (Fig. 1B) shows that there is an interstitial layer between STO and FeSe films. Similar interfacial structures were reported (17, 38). The room temperature EELS study on FeSe/STO system (17) identified the layer as two TiO_x layers with increased oxygen vacancies. A “tail-frame” like structure was observed in the study of Li *et al.* (17) and was speculated by the authors as an extra Se layer. Our atomically resolved HAADF-STEM imaging and EELS measurements collect simultaneously Ti, Fe, and Se edge signals (Fig. 1, B to D, and fig. S2) and clearly reveal the Se layer (labeled as Se1 in Fig. 1B) between the double TiO_x layers and the FeSe layer. Although careful EELS experiments indicate a trace of Ti and Fe signals in this layer, analysis of core-loss delocalization (39) suggests that the signals come from the neighboring Ti and Fe atomic columns and are localized within one atomic layer. This Se layer may play a role in binding the double TiO_x layer to the STO (40), otherwise the double TiO_x layer on the surface is not stable and tends to unbind from the STO surface. The overall structure of the FeSe film on STO is schematically shown in Fig. 1A.

Figure 1 (G to J) shows the superconducting transitions of the S1 (1 UC), S2 (2 UC), and S3 (8 UC) films shifting to higher temperature with increasing backgate voltage V_g , whereas the S4 (14 UC) film shows weak gate dependence. T_c is defined as the temperature of zero resistance (specifically when the measured resistance is lower than 0.5% of the normal state value), and we also list $T_{c\text{-mid}}$ as the temperature

when the resistance has dropped to half of the normal state value. For the S1 (1 UC) film (Fig. 1G), the T_c 's are 15.2, 19.0, and 21.5 K, and the $T_{c\text{-mid}}$'s are 21.8, 24.9, and 27.0 K at $V_g = -200, 0,$ and $+200$ V, respectively. The T_c (or $T_{c\text{-mid}}$) found here for the S1 (1UC) film is substantially lower than that reported in STM (9), ARPES (5–7), and in situ transport studies (14). The fact that the FeTe capping layer introduces hole carriers into the FeSe film is the likely reason for reducing T_c (fig. S10).

EELS measurement results

Figure 2 (A to C) shows the core-loss EELS mapping with energy (in eV) as the horizontal axis and the spatial position along the thickness direction as the vertical axis for the same S1 (1 UC), S3 (8 UC), and S4 (14 UC) films. A blue shift of the Fe's L_3 edge extending into the FeSe film from the STO interface is observed in all three samples at 10 K (Fig. 2, D to F) but is not seen at 300 K (fig. S4). For the 8- and 14-UC films, the observed energy shift extends beyond 1 UC but less than 2 UC, and smoothly diminishes into FeSe film. The maximum magnitudes of the blue shift at the interface shown for the 8- and 14-UC films are $\sim 0.7 \pm 0.1$ eV (Fig. 2E) and $\sim 0.4 \pm 0.1$ eV (Fig. 2F), respectively. For the 1-UC film, the blue shift is clearly present (Fig. 2D), but the magnitude is hard to estimate. This limited energy and spatial resolution for the 1-UC film is the result of signal delocalization and probe broadening.

To understand the origin of the energy shift, we performed Green's function-based EELS spectral simulation using the program FEF (41–43). The local chemical environment of the FeSe films will change when it is in direct proximity with STO surface. However, this effect can be excluded as the origin of the shift because no energy shift is found in the main Fe's L_3 in the simulation, even for the Fe ions at the first UC closest to STO (Fig. 2G). The effect of STO shows up as a shoulder in the spectrum on the high energy side of the main peak near 712 eV. The

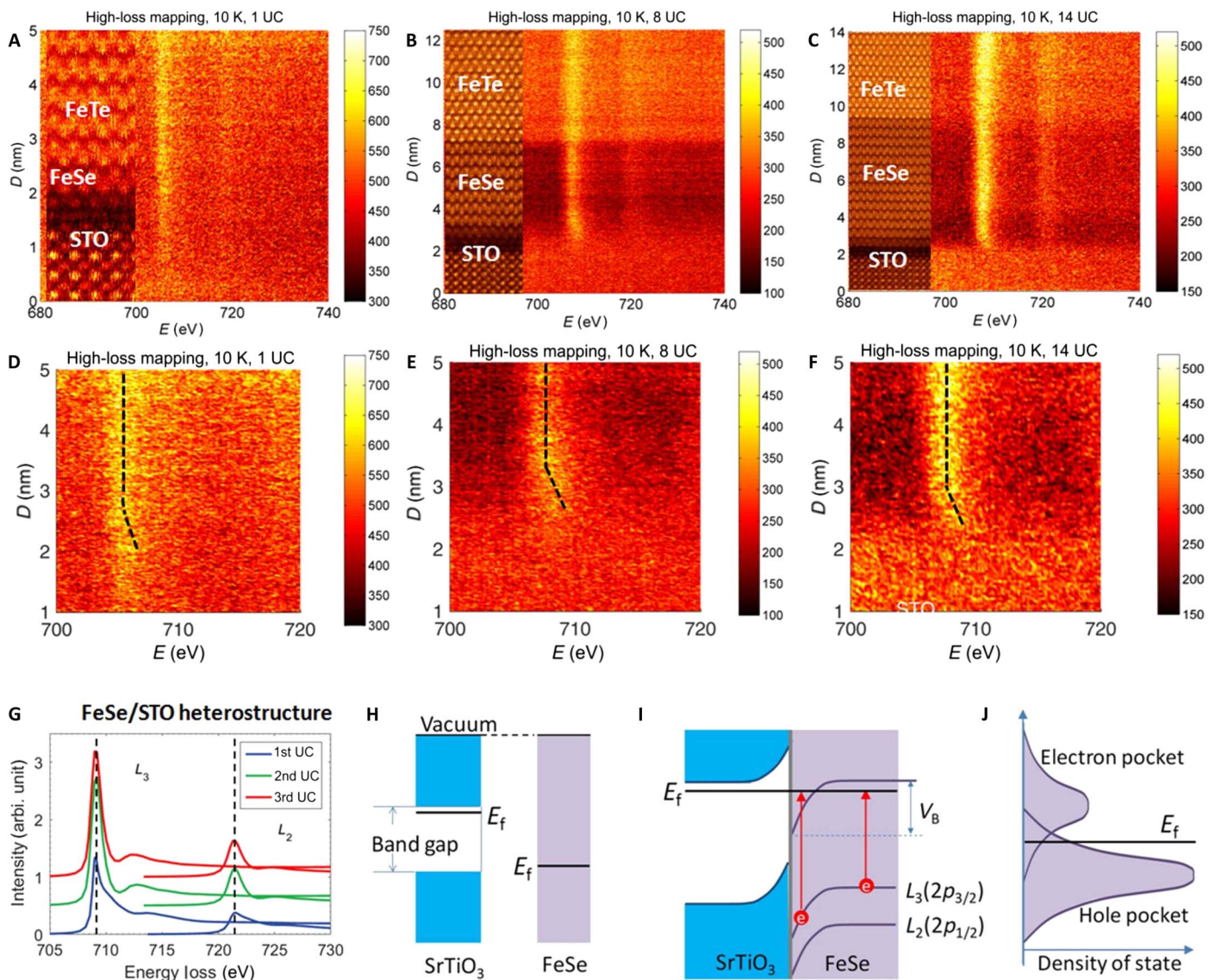


Fig. 2. Atomically resolved STEM-EELS results at 10 K. (A to C) Core-loss EELS mapping with an energy range between 680 and 740 eV for (A) S1 (1 UC), (B) S3 (8 UC), and (C) S4 (14 UC). (D to F) The zoomed-in images at the interface region in (A) to (C), respectively. The dash lines are shown as guides for eyes. (G) FEFF simulation of the core-loss EELS spectra using the super cell in Fig. 1A. (H) Schematic of work function difference between STO and FeSe. (I) Schematics of screening potential profiles in the FeSe region induced by electron transfer from the proximal STO interface. Because of the finite screening length, Fe's $L_3(2p_{3/2})$ and $L_2(2p_{1/2})$ levels close to the interface bend accordingly, giving a blue shift of the electron energy loss. V_B is total potential variation. (J) At the interface, density of states (DOSs) of hole pocket is higher than that of electron pocket. It needs more electrons to fill up the hole pocket as compared with electron pocket for the same E_f shift.

shoulders found at the second and third UC are nearly identical. The strain effect can also be excluded because FeSe is experiencing tensile stress near STO (6), which should result in a red shift instead of the observed blue shift (fig. S6).

We propose that the screening potential in the first two FeSe layers near the interface, induced by transferred electrons from the STO substrate to FeSe layers, is responsible for the observed blue shift. The STO substrates used in the experiments are electron-doped due to oxygen vacancies at the TiO_x interstitial layer between STO and FeSe films (6, 17, 23). The electrons that reside in impurity bands are typically close to the bottom of the STO conduction bands, although the Fermi level in FeSe is close to the maximum of the STO valence band (22). This is schematically shown in Fig. 2H. Consequently, the work function

difference between FeSe and STO is close to the STO band gap (~ 3 eV) and can lead to a charge transfer from STO to FeSe. The built-in electric field induced by this charge transfer yields a potential across the FeSe/STO interface (Fig. 2I). Given the metallic nature of FeSe films, this potential can be regarded as the screening potential with a screening length of 2 UC. Because of the finite screening length, the energy difference between the energy of Fe $L_3(2p_{3/2})$ and $L_2(2p_{1/2})$ levels near the interface and the Fermi energy is increased, giving rise to the blue-shift spectra of these core levels in the electron energy loss. The screening potential picture also provides an explanation of the higher energy shift observed in the 8-UC film than that in the 14-UC film (~ 0.7 eV versus ~ 0.4 eV). Our Hall transport measurements (Fig. 3) show more hole-type carriers in the 14-UC film as compared to those

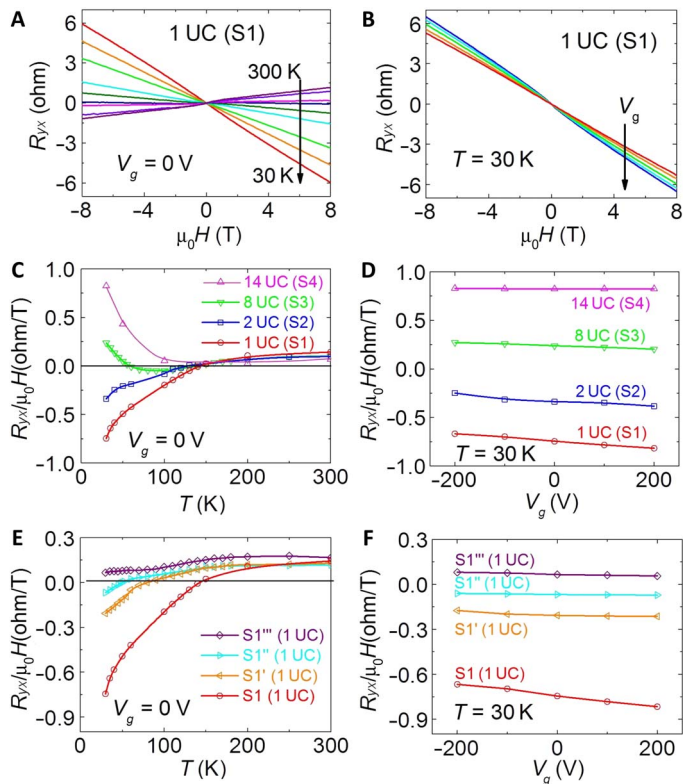


Fig. 3. Hall transport studies on FeSe/STO samples. (A) R_{yx} versus μ_0H at $V_g = 0$ V at different temperatures from 300 to 30 K for the S1 (1 UC) film. (B) R_{yx} versus μ_0H at $T = 30$ K at different gate voltages ranging from -200 to $+200$ V for the S1 (1 UC) film. (C) R_H as function of T at $V_g = 0$ V for the S1 (1 UC), S2 (2 UC), S3 (8 UC), and S4 (14 UC) films. (D) R_H as function of V_g at $T = 30$ K for the S1 (1 UC), S2 (2 UC), S3 (8 UC), and S4 (14 UC) films. (E) R_H as function of T under $V_g = 0$ V for S1 (1 UC), S1' (1 UC), S1'' (1 UC), and S1''' (1 UC) annealed at different temperatures. (F) R_H as a function of V_g at $T = 30$ K for S1 (1 UC), S1' (1 UC), S1'' (1 UC), and S1''' (1 UC).

in the 8-UC film, suggesting a lower Fermi energy E_F in the thicker film. According to first-principles calculations on a FeSe film (24), the DOS increases when the Fermi energy is lowered deep into the valence band (Fig. 2J). Thus, we expect a smaller DOS at the Fermi energy for the thinner film and larger energy shift with the assumption that same numbers of electrons were transferred. To arrive at a more quantitative estimate, we make the following assumptions: (i) The transferred charges are assumed to be uniformly distributed in the FeSe layers with a thickness d around 1 to 2 UC (0.55 to 1.1 nm) near the interface, (ii) all the transferred electrons come from 2DEG on the STO (001) surface (44, 45) with a sheet carrier density $n \sim 0.5$ to 1.5×10^{14} cm $^{-2}$, and (iii) the dielectric constant of the FeSe film $\epsilon_{\text{FeSe}} \sim 15$ (25). These simplifications lead to an estimate of the voltage drop V_B between 0.1 and 1 V according to the equation $V_B = \frac{en \cdot d}{2\epsilon_{\text{FeSe}}}$. This is consistent with the observed energy shift (8 UC, ~ 0.7 eV; 14 UC, ~ 0.4 eV). This consistency supports the conclusion that the blue shifts observed in the EELS core-loss mapping are direct evidence of electron transfer from STO to the FeSe films.

Hall transport results

In addition to longitudinal transport and EELS measurements, we carried out Hall transport measurements systematically under differ-

ent magnetic field (μ_0H), T , and V_g on S1 (1 UC), S3 (8 UC), S4 (14 UC), S2 (2 UC), and also on the three 1-UC films (S1', S1'', and S1''') annealed at lower temperatures (Fig. 3 and fig. S8). The Hall resistances R_{yx} were measured as a function of μ_0H from -8 to 8 T at different fixed T ranging from 300 K down to 30 K. Linear dependence of R_{yx} on μ_0H is found for all samples, consistent with the Hall results in the study of Sun *et al.* (12). The T dependences of the Hall coefficient $R_H = R_{yx}/\mu_0H$ for all seven samples are shown in Fig. 3 (C and E). R_H changes sign from positive to negative upon cooling from 300 to ~ 140 K for S1 (1 UC), S2 (2 UC), and S3 (8 UC) films. This behavior has been observed in other multiband materials in the presence of both electron-type and hole-type carriers, such as NbSe $_2$ (46). Below 50 K, R_H of the S3 (8 UC) film turns positive again. R_H for the S4 (14 UC) film stays positive for all temperatures with a rapid increase below 100 K. This behavior indicates that the hole carrier densities n_h in both 8- and 14-UC FeSe films are enhanced substantially at low T (see the Supplementary Materials). This hole carrier-dominated behavior for the thicker film is similar to that found for bulk FeSe with low T_c . The onset temperature of superconductivity in 8-UC FeSe films is higher than T_c of bulk FeSe (1, 2), indicating that the interface is still responsible for the superconductivity of 8-UC FeSe film. Figure 3E shows that annealing at higher temperatures makes the 1-UC films to be more electron carrier dominant at low T and as a consequence with higher T_c as shown in Fig. 1E.

The V_g dependence of R_H for all seven samples has been studied. R_{yx} versus μ_0H at 30 K for the S1 (1 UC) film under different V_g is shown in fig. 3B, and additional data for other samples are shown in fig. S8. Figure 3D shows that the effect on R_H due to a change in V_g from -200 to $+200$ V is an order of magnitude smaller than the difference in R_H of films of different thicknesses. Similarly, weak dependences of R_H on gating are also seen for the four 1-UC samples subjected to different annealing procedures (Fig. 3F).

The relationship between R_H and the carrier density (which depends on V_g) in our samples is in sharp contrast to that in a typical metal, where R_H is inversely proportional to carrier density. This is the case because our samples are populated by both electron- and hole-type carriers. In other words

$$R_H = \frac{n_h \mu_h^2 - n_e \mu_e^2}{e(n_h \mu_h + n_e \mu_e)^2} \quad (1)$$

where e is the electron charge, n_h and n_e are the hole and electron carrier densities, and μ_h and μ_e are the hole and electron mobilities. According to Eq. 1, when $n_e \mu_e^2 > n_h \mu_h^2 > n_e \mu_e^2 / (2 + \mu_e / \mu_h)$, both $\frac{\partial R_H}{\partial n_e} < 0$ and $R_H < 0$ are satisfied.

Similar T_c but different R_{yx} is observed for samples S3 and S1'. This is related to the fact that the transferred charge from STO is found only in the first 1- to 2-UC FeSe close to the interface. It is likely that the electron density at the interface for S3 and S1' are very similar, but sample S3 (8 UC) has more hole carriers than the sample S1' (1 UC). Therefore, sample S3 shows a positive R_H , whereas sample S1' shows a negative R_H .

DISCUSSION

In Fig. 4, we summarize the effect of annealing, film thickness variation, and V_g on $T_{c\text{-mid}}$ and R_H of the seven samples. Although R_H and $T_{c\text{-mid}}$ of the film depends on both the thickness and the annealing

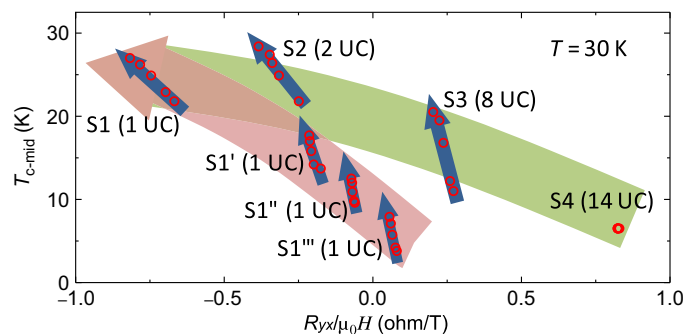


Fig. 4. The superconducting transition temperature $T_{c\text{-mid}}$ as a function of the Hall coefficient R_H at 30 K. The different samples in our study are represented by blue arrows. The red circles show $T_{c\text{-mid}}$ and R_H values, from bottom to top, at V_g 's of -200 , -100 , 0 , 100 , and 200 V. The broad pink arrow groups the 1-UC films annealed at different temperatures 550° , 500° , 400° , and 330°C , respectively, and the green arrow groups samples with different thicknesses annealed at 550°C . The slopes of the blue circles (which summarize the backgating effect) are much steeper than the slopes of the green and pink arrows. This means that backgating is particularly effective in enhancing T_c for thin FeSe films with minimal effect in R_H . Plots using R_H at 40 and 50 K in the Supplementary Materials show similar conclusions.

temperature, backgating from STO is found to be particularly effective in enhancing the $T_{c\text{-mid}}$ of thin FeSe films without significantly changing R_H , aka the total carrier density of the film. This is the case because, as we have shown in presenting the EELS results, there is already a 2DEG confined near the interface transferred from STO. Because FeSe film is a metal, the accumulated charges by the gating effect is much smaller compared to carrier density in the system. The accumulated electron density at the interface at $V_g = +200$ V is estimated to be $1.84 \times 10^{13} \text{ cm}^{-2}$ at 30 K based on the dielectric constant value of 8300 (47). This is more than five times smaller than the density of the 2DEG found on the STO (001) surface (44, 45), namely, $n \sim 1 \times 10^{14} \text{ cm}^{-2}$. In other words, the electric field generated by the backgate is screened by the accumulated charges at the STO/FeSe interface, and its effect is limited within the screening length. Thus, we suggest that the main influence of the backgate on T_c is to pull electrons in FeSe films closer to the STO interface. At the FeSe/STO interface, electrons can benefit from the high Debye temperature STO phonon bath and thus the electron-phonon coupling for superconductivity is enhanced (7, 19, 21, 48–50). This enhancement scales with the product $[-N(0)|g(k,q)|^2]$, where $N(0)$ is the DOS and $g(k,q)$ is the coupling vortex (51). Our results cannot single out whether it is $N(0)$ or $g(k,q)$ that is primarily responsible for the enhancement of electron-phonon coupling. It was pointed out by B. Li *et al.* in a calculation (24) that a charge transfer process will enhance DOS. Because the transferred electrons are close to the STO surface, it is possible that $g(k,q)$ is also increased.

Besides electron-phonon coupling between the FeSe film and the STO substrate, the electron-electron correlation within the film due to the transferred charges across the interface can also be enhanced and lead to an enhanced T_c . However, a theoretical study (37) found a reduction of correlations in the FeSe monolayer on STO without oxygen vacancies as compared with bulk FeSe. When the same reference considers the FeSe/STO system with oxygen vacancies, mimicking the actual experimental situation, the Fermi surface is altered, and a strong correlation is found in the FeSe monolayer. Therefore, we arrive at the conclusion that the transfer of electrons from STO across the interface into the FeSe film can enhance both electron coupling to STO phonons

and electron-electron interaction within the FeSe film. Both mechanisms can be responsible for the observed T_c enhancement in the FeSe/STO system.

Figure 1 (G to I) shows obvious $T_{c\text{-mid}}$ dependence on V_g for 1-, 2-, and 8-UC films with the 8-UC film showing the strongest effect. This dependence is not seen for the 14-UC film (Fig. 1J). We found the gating effect does become stronger with decreasing temperature possibly due to the strong temperature dependence of the dielectric constant of STO (fig. S9) (52), indicating that in the 8-UC film (and also S1', S1'', and S1''') with lower $T_{c\text{-mid}}$, the gating effect may thus be enhanced to provide more doping carriers in the 8-UC film. The asymmetric potential induced by the V_g could be another reason for the strong V_g effect for the 1- and 2-UC films to 8-UC film. A positive V_g tends to pull the electron carriers to the FeSe layers closer to the STO/FeSe interface and “repulse” hole carriers away from the interface. This spatial separation between electron and hole carriers has a strong influence on the critical temperature $T_{c\text{-mid}}$, as well as the curvature of R_{xx} around $T_{c\text{-mid}}$. The length scale of spatial separation is determined by the screening length, which is on the order of 1 to 2 UC. This screening effect is particularly strong for the 8-UC film because the film thickness is larger than the screening length. However, for the 1- or 2-UC film, the strong quantum confinement will significantly reduce the spatial separation between electron and hole carriers, thus weakening the effect. Because the 14-UC film is also thicker than the screening length, the mechanism of spatial separation of charges should be similar to the 8-UC film. The reason why there is no observable gating effect for the 14-UC film may be related to the fact that the high hole carrier concentration in the thicker, that is, bulk-like, films overwhelms the spatial separation effect operable in thinner films.

To summarize, we carried out a complementary electrical transport and low-temperature EELS measurements to understand the physics of the extraordinary high T_c of interface superconductivity in FeSe/STO system. Our results show direct evidence of electrons transferred from STO to the first two atomic layers of FeSe films. The confinement at the interface enhances the electron-electron interaction within the FeSe film and also strengthens the coupling of the electrons to the STO phonons, thus elevating T_c . Our new technique of EELS mapping across the FeSe/SrTiO₃ interface at cryogenic temperature can be a powerful tool for the study of other 2D systems.

Note that during the peer-review process of this paper, an independent work with a similar conclusion but different techniques has appeared in *Nature Communications* (53).

MATERIALS AND METHODS

MBE growth

Thin film growth for transport measurement was performed using a custom-built ultrahigh vacuum (UHV) MBE system with a base pressure lower than 5×10^{-10} torr. Before the STO substrate was loaded into the MBE chamber, it was annealed in a tube furnace at 985°C under flowing oxygen gas. The TiO₂-terminated STO surface was formed during this heat treatment process (8). Then, the heat-treated STO substrates were transferred into the UHV MBE chamber and annealed at 600°C for 1 hour. Oxygen vacancies on the surface, that is, the TiO_x double layer, were likely formed at this stage. FeSe films were grown by co-evaporating Fe (99.995%) from an E-gun cell and Se (99.999%) from a Knudsen cell with a flux ratio of 1:20 on the STO substrate at 330°C . The fluxes of the Fe and Se were determined using separate quartz

crystal monitors. The growth rate for the films was approximately 0.2 UC/min. Epitaxial growth was monitored by in situ reflective high-energy electron diffraction (RHEED), where the high crystal quality and the atomically flat surface were confirmed by the streaky and sharp “1 × 1” patterns (fig. S1). The annealing temperatures for S1 (1 UC), S1' (1 UC), S1'' (1 UC), and S1''' (1 UC) are 550°, 500°, 400°, and 330°C, respectively. A 14-UC-thick FeTe capping layer is deposited on the FeSe films at ~330°C, and then, the sample was cooled down to room temperature. To further protect the FeSe films, we deposited a 10-nm-thick Te layer at room temperature on top of the FeTe layer before its removal from the MBE chamber for transport measurements.

Atomic imaging and EELS measurements

The low temperature EELS measurements were carried out using a custom-designed, low-drift liquid-He stage newly developed by Gatan for atomic imaging and spectroscopy. The temperature is monitored by a factory-calibrated silicone diode. The spatial increment of the line scan of the spectrum images was ~0.02 nm. Both low-loss, including the zero-loss peak, and core-loss spectra were collected simultaneously for precise calibration to obtain the precise energy shift.

Transport measurements

The Hall and longitudinal resistances were carried out in a Quantum Design Physical Property Measurement System (1.8 K, 9 T) with the excitation current flowing in the film plane and the magnetic field applied perpendicular to the plane. The FeSe/STO films were scratched to a six-terminal Hall bar geometry device using a needle by hands. The effective area of the Hall bar device is ~1 mm × 0.5 mm. All the longitudinal resistances in the manuscript and supporting materials were expressed as sheet resistances. The backgate voltage was applied using the Keithley 2450 from –200 to +200V.

EELS simulations

The EELS simulation is carried out using FEFF 9, which is a software package to perform multiple scattering calculations of multiple atomic core-level spectroscopies including EXAFS and EELS. A part of the atomic structure used for this simulation is shown in Fig. 1A, where both the TiO₂ double layer and the additional Se layer were incorporated into the simulation. The atomic structure was optimized on the basis of energy potential method, where the distance between the additional Se layer and the TiO₂ double layer appears to be smaller than that from transmission electron microscopy observation in Fig. 1B. We changed the distance between the FeSe and the STO layer and found negligible effect on the Fe L₃ and L₂ energy level positions, and no blue shift was observed. The full multiple scattering cutoff radius and the self-consistent-field cutoff radius were taken as 0.8 and 0.4 nm to ensure the convergence. The supercell size is chosen to be 10-UC FeSe and STO, far beyond the cutoff radii. Moreover, the Hedin-Lundqvist self-energy and the random phase approximation with core-hole correction were taken into account properly in the simulation.

SUPPLEMENTARY MATERIALS

Supplementary material for this article is available at <http://advances.sciencemag.org/cgi/content/full/4/3/eaao2682/DC1>

fig. S1. RHEED patterns.

fig. S2. EELS spectrum image analysis for the 1-UC FeSe/SrTiO₃ interface.

fig. S3. EELS spectra at three different spatial locations (first FeSe layer in proximity to STO, FeSe film 4 UC away from STO, and FeTe layer region for 8- and 14-UC FeSe/STO films).

fig. S4. Core-loss EELS mappings across the FeSe/STO interface of the 1- (S1), 8- (S3), and 14-UC (S4) films at room temperature.

fig. S5. Low-loss EELS mappings across the interface of the 1- (S1), 8- (S3), and 14-UC (S4) films.
fig. S6. FEFF simulation of the core-loss EELS spectra in the first UC FeSe layer near STO with and without tensile stress.

fig. S7. Evolution of R_{xx} versus T with gate voltage under different magnetic field for all seven samples S1, S2, S3, S4, S1', S1'', and S1'''.

fig. S8. Hall transport results for all seven samples S1, S2, S3, S4, S1', S1'', and S1'''.

fig. S9. Evolution of R_{xx} versus μ_0H at various gate voltages at 40 and 50 K in sample S1.

fig. S10. The superconducting transition temperature T_{c-mid} as a function of the Hall coefficient R_H measured at 40 K and 50 K.

fig. S11. Transport results of a 14-UC FeTe film on SrTiO₃ substrate.

References (54–56)

REFERENCES AND NOTES

1. F.-C. Hsu, J.-Y. Luo, K.-W. Yeh, T.-K. Chen, T.-W. Huang, P. M. Wu, Y.-C. Lee, Y.-L. Huang, Y.-Y. Chu, D.-C. Yan, M.-K. Wu, Superconductivity in the PbO-type structure α -FeSe. *Proc. Natl. Acad. Sci. U.S.A.* **105**, 14262–14264 (2008).
2. Y. J. Song, J. B. Hong, B. H. Min, Y. S. Kwon, K. J. Lee, M. H. Jung, J.-S. Rhyee, Superconducting properties of a stoichiometric FeSe compound and two anomalous features in the normal state. *J. Korean Phys. Soc.* **59**, 312–316 (2011).
3. Q.-Y. Wang, Z. Li, W.-H. Zhang, Z.-C. Zhang, J.-S. Zhang, W. Li, H. Ding, Y.-B. Ou, P. Deng, K. Chang, J. Wen, C.-L. Song, K. He, J.-F. Jia, S.-H. Ji, Y.-Y. Wang, L.-L. Wang, X. Chen, X.-C. Ma, Q.-K. Xue, Interface-induced high-temperature superconductivity in single unit-cell FeSe films on SrTiO₃. *Chinese Phys. Lett.* **29**, 037402 (2012).
4. D. F. Liu, W. H. Zhang, D. X. Mou, J. F. He, Y.-B. Ou, Q.-Y. Wang, Z. Li, L. L. Wang, L. Zhao, S. L. He, Y. Y. Peng, X. Liu, C. Y. Chen, L. Yu, G. D. Liu, X. L. Dong, J. Zhang, C. T. Chen, Z. Y. Xu, J. P. Hu, X. Chen, X. C. Ma, Q. K. Xue, X. J. Zhou, Electronic origin of high-temperature superconductivity in single-layer FeSe superconductor. *Nat. Commun.* **3**, 931 (2012).
5. S. L. He, J. F. He, W. H. Zhang, L. Zhao, D. F. Liu, X. Liu, D. X. Mou, Y.-B. Ou, Q.-Y. Wang, Z. Li, L. L. Wang, Y. Y. Peng, Y. Liu, C. Y. Chen, L. Yu, G. D. Liu, X. L. Dong, J. Zhang, C. T. Chen, Z. Y. Xu, X. Chen, X. Ma, Q. K. Xue, X. J. Zhou, Phase diagram and electronic indication of high-temperature superconductivity at 65 K in single-layer FeSe films. *Nat. Mater.* **12**, 605–610 (2013).
6. S. Y. Tan, Y. Zhang, M. Xia, Z. R. Ye, F. Chen, X. Xie, R. Peng, D. F. Xu, Q. Fan, H. C. Xu, J. Jiang, T. Zhang, X. C. Lai, T. Xiang, J. P. Hu, B. P. Xie, D. L. Feng, Interface-induced superconductivity and strain-dependent spin density waves in FeSe/SrTiO₃ thin films. *Nat. Mater.* **12**, 634–640 (2013).
7. J. J. Lee, F. T. Schmitt, R. G. Moore, S. Johnston, Y.-T. Cui, W. Li, M. Yi, Z. K. Liu, M. Hashimoto, Y. Zhang, D. H. Lu, T. P. Devereaux, D.-H. Lee, Z.-X. Shen, Interfacial mode coupling as the origin of the enhancement of T_c in FeSe films on SrTiO₃. *Nature* **515**, 245–248 (2014).
8. W.-H. Zhang, Y. Sun, J.-S. Zhang, F.-S. Li, M.-H. Guo, Y.-F. Zhao, H.-M. Zhang, J.-P. Peng, Y. Xing, H.-C. Wang, T. Fujita, A. Hirata, Z. Li, H. Ding, C.-J. Tang, M. Wang, Q.-Y. Wang, K. He, S.-H. Ji, X. Chen, J.-F. Wang, Z.-C. Xia, L. Li, Y.-Y. Wang, J. Wang, L.-L. Wang, M.-W. Chen, Q.-K. Xue, X.-C. Ma, Direct observation of high-temperature superconductivity in one-unit-cell FeSe films. *Chinese Phys. Lett.* **31**, 017401 (2014).
9. W. H. Zhang, Z. Li, F. S. Li, H. M. Zhang, J. P. Peng, C. J. Tang, Q. Y. Wang, K. He, X. Chen, L. L. Wang, X. C. Ma, Q.-K. Xue, Interface charge doping effects on superconductivity of single-unit-cell FeSe films on SrTiO₃ substrates. *Phys. Rev. B* **89**, 060506 (2014).
10. X. Liu, D. F. Liu, W. H. Zhang, J. F. He, L. Zhao, S. L. He, D. X. Mou, F. S. Li, C. J. Tang, Z. Li, L. L. Wang, Y. Y. Peng, Y. Liu, C. Y. Chen, L. Yu, G. D. Liu, X. L. Dong, J. Zhang, C. T. Chen, Z. Y. Xu, X. Chen, X. C. Ma, Q. K. Xue, X. J. Zhou, Dichotomy of the electronic structure and superconductivity between single-layer and double-layer FeSe/SrTiO₃ films. *Nat. Commun.* **5**, 5047 (2014).
11. R. Peng, H. C. Xu, S. Y. Tan, H. Y. Cao, M. Xia, X. P. Shen, Z. C. Huang, C. H. P. Wen, Q. Song, T. Zhang, B. P. Xie, X. G. Gong, D. L. Feng, Tuning the band structure and superconductivity in single-layer FeSe by interface engineering. *Nat. Commun.* **5**, 5044 (2014).
12. Y. Sun, W. H. Zhang, Y. Xing, F. S. Li, Y. F. Zhao, Z. C. Xia, L. L. Wang, X. C. Ma, Q.-K. Xue, J. Wang, High temperature superconducting FeSe films on SrTiO₃ substrates. *Sci. Rep.* **4**, 6040 (2014).
13. L. Z. Deng, B. Lv, Z. Wu, Y. Y. Xue, W. H. Zhang, F. S. Li, L. L. Wang, X. C. Ma, Q. K. Xue, C. W. Chu, Meissner and mesoscopic superconducting states in 1–4 unit-cell FeSe films. *Phys. Rev. B* **90**, 214513 (2014).
14. J.-F. Ge, Z.-L. Liu, C. Liu, C.-L. Gao, D. Qian, Q.-K. Xue, Y. Liu, J.-F. Jia, Superconductivity above 100 K in single-layer FeSe films on doped SrTiO₃. *Nat. Mater.* **14**, 285–289 (2015).

15. Q. Fan, W. H. Zhang, X. Liu, Y. J. Fan, M. Q. Ren, R. Peng, H. C. Xu, B. P. Xie, J. P. Hu, T. Zhang, D. L. Feng, Plain *s*-wave superconductivity in single-layer FeSe on SrTiO₃ probed by scanning tunnelling microscopy. *Nat. Phys.* **11**, 946–952 (2015).
16. D. Huang, C.-L. Song, T. A. Webb, S. Fang, C.-Z. Chang, J. S. Moodera, E. Kaxiras, J. E. Hoffman, Revealing the empty-state electronic structure of single-unit-cell FeSe/SrTiO₃. *Phys. Rev. Lett.* **115**, 017002 (2015).
17. F. S. Li, Q. H. Zhang, C. J. Tang, C. Liu, J. N. Shi, C. N. Nie, G. Y. Zhou, Z. Li, W. H. Zhang, C.-L. Song, K. He, S. H. Ji, S. B. Zhang, L. Gu, L. L. Wang, X.-C. Ma, Q.-K. Xue, Atomically resolved FeSe/SrTiO₃(001) interface structure by scanning transmission electron microscopy. *2D Mater.* **3**, 024002 (2016).
18. W. W. Zhao, C.-Z. Chang, X. X. Xi, K. F. Mak, J. S. Moodera, Vortex phase transitions in monolayer FeSe film on SrTiO₃. *2D Mater.* **3**, 024006 (2016).
19. S. Zhang, J. Guan, X. Jia, B. Liu, W. Wang, F. Li, L. Wang, X. Ma, Q. Xue, J. Zhang, E. W. Plummer, X. Zhu, J. Guo, The role of SrTiO₃ phonon penetrating into thin FeSe films in the enhancement of superconductivity. arXiv:1605.06941v2 (2016).
20. Q. Wang, W. Zhang, Z. Zhang, Y. Sun, Y. Xing, Y. Wang, L. Wang, X. Ma, Q.-K. Xue, J. Wang, Thickness dependence of superconductivity and superconductor-insulator transition in ultrathin FeSe films on SrTiO₃(001) substrate. *2D Mater.* **2**, 044012 (2015).
21. Y.-Y. Xiang, F. Wang, D. Wang, Q.-H. Wang, D.-H. Lee, High-temperature superconductivity at the FeSe/SrTiO₃ interface. *Phys. Rev. B* **86**, 134508 (2012).
22. K. Liu, Z.-Y. Lu, T. Xiang, Atomic and electronic structures of FeSe monolayer and bilayer thin films on SrTiO₃ (001): First-principles study. *Phys. Rev. B* **85**, 235123 (2012).
23. J. Bang, Z. Li, Y. Y. Sun, A. Samanta, Y. Y. Zhang, W. H. Zhang, L. L. Wang, X. Chen, X. C. Ma, Q. K. Xue, S. B. Zhang, Atomic and electronic structures of single-layer FeSe on SrTiO₃(001): The role of oxygen deficiency. *Phys. Rev. B* **87**, 220503 (2013).
24. B. Li, Z. W. Xing, G. Q. Huang, D. Y. Xing, Electron-phonon coupling enhanced by the FeSe/SrTiO₃ interface. *J. Appl. Phys.* **115**, 193907 (2014).
25. Y. Zhou, A. J. Millis, Charge transfer and electron-phonon coupling in monolayer FeSe on Nb doped SrTiO₃. arXiv:1603.02728v1 (2016).
26. T. Berlijn, H. P. Cheng, P. J. Hirschfeld, W. Ku, Doping effects of Se vacancies in monolayer FeSe. *Phys. Rev. B* **89**, 020501 (2014).
27. V. Mishra, D. J. Scalapino, T. A. Maier, *s_x* pairing near a Lifshitz transition. *Sci. Rep.* **6**, 32078 (2016).
28. A. Linscheid, S. Maiti, Y. Wang, S. Johnston, P. J. Hirschfeld, High *T_c* via spin fluctuations from incipient bands: Application to monolayers and intercalates of FeSe. *Phys. Rev. Lett.* **117**, 077003 (2016).
29. Y. Miyata, K. Nakayama, K. Sugawara, T. Sato, T. Takahashi, High-temperature superconductivity in potassium-coated multilayer FeSe thin films. *Nat. Mater.* **14**, 775–779 (2015).
30. C.-L. Song, H.-M. Zhang, Y. Zhong, X.-P. Hu, S.-H. Ji, L. Wang, K. He, X.-C. Ma, Q.-K. Xue, Observation of double-dome superconductivity in potassium-doped FeSe thin films. *Phys. Rev. Lett.* **116**, 157001 (2016).
31. J. Shiogai, Y. Ito, T. Mitsuhashi, T. Nojima, A. Tsukazaki, Electric-field-induced superconductivity in electrochemically etched ultrathin FeSe films on SrTiO₃ and MgO. *Nat. Phys.* **12**, 42–46 (2016).
32. B. Lei, J. H. Cui, Z. J. Xiang, C. Shang, N. Z. Wang, G. J. Ye, X. G. Luo, T. Wu, Z. Sun, X. H. Chen, Evolution of high-temperature superconductivity from a low-*T_c* phase tuned by carrier concentration in FeSe thin flakes. *Phys. Rev. Lett.* **116**, 077002 (2016).
33. C. J. Tang, D. Zhang, Y. Y. Zang, C. Liu, G. Y. Zhou, Z. Li, C. Zheng, X. P. Hu, C. L. Song, S. H. Ji, K. He, X. Chen, L. L. Wang, X. C. Ma, Q.-K. Xue, Superconductivity dichotomy in K-coated single and double unit cell FeSe films on SrTiO₃. *Phys. Rev. B* **92**, 180507 (2015).
34. A. Tamai, A. Y. Ganin, E. Rozbicki, J. Bacsá, W. Meevasana, P. D. C. King, M. Caffio, R. Schaub, S. Margadonna, K. Prassides, M. J. Rosseinsky, F. Baumberger, Strong electron correlations in the normal state of the iron-based FeSe_{0.42}Te_{0.58} superconductor observed by angle-resolved photoemission spectroscopy. *Phys. Rev. Lett.* **104**, 097002 (2010).
35. Z. P. Yin, K. Haule, G. Kotliar, Kinetic frustration and the nature of the magnetic and paramagnetic states in iron pnictides and iron chalcogenides. *Nat. Mater.* **10**, 932–935 (2011).
36. Y. Imai, Y. Sawada, F. Nabeshima, A. Maeda, Suppression of phase separation and giant enhancement of superconducting transition temperature in FeSe_{1-x}Te_x thin films. *Proc. Natl. Acad. Sci. U.S.A.* **112**, 1937–1940 (2015).
37. S. Mandal, P. Zhang, S. Ismail-Beigi, K. Haule, How correlated is the FeSe/SrTiO₃ system? *Phys. Rev. Lett.* **119**, 067004 (2017).
38. H. F. Hu, J.-H. Kwon, M. Zheng, C. Zhang, L. H. Greene, J. N. Eckstein, J.-M. Zuo, Impact of interstitial oxygen on the electronic and magnetic structure in superconducting Fe_{1+y}TeO_x thin films. *Phys. Rev. B* **90**, 180504 (2014).
39. K. Kimoto, T. Asaka, T. Nagai, M. Saito, Y. Matsui, K. Ishizuka, Element-selective imaging of atomic columns in a crystal using STEM and EELS. *Nature* **450**, 702–704 (2007).
40. A. Linscheid, Electronic properties of the FeSe/STO interface from first-principle calculations. *Supercond. Sci. Technol.* **29**, 104005 (2016).
41. J. J. Rehr, J. J. Kas, M. P. Prange, A. P. Sorini, Y. Takimoto, F. Vila, Ab initio theory and calculations of X-ray spectra. *C. R. Phys.* **10**, 548–559 (2009).
42. J. J. Rehr, J. J. Kas, F. D. Vila, M. P. Prange, K. Jorissen, Parameter-free calculations of X-ray spectra with FEFF9. *Phys. Chem. Chem. Phys.* **12**, 5503–5513 (2010).
43. M. D. Li, C.-Z. Chang, L. J. Wu, J. Tao, W. W. Zhao, M. H. W. Chan, J. S. Moodera, J. Li, Y. M. Zhu, Experimental verification of the van Vleck nature of long-range ferromagnetic order in the vanadium-doped three-dimensional topological insulator Sb₂Te₃. *Phys. Rev. Lett.* **114**, 146802 (2015).
44. A. F. Santander-Syro, O. Copie, T. Kondo, F. Fortuna, S. Pailhès, R. Weht, X. G. Qiu, F. Bertran, A. Nicolaou, A. Taleb-Ibrahimi, P. Le Fèvre, G. Herranz, M. Bibes, N. Reyren, Y. Apertet, P. Lecoeur, A. Barthélémy, M. J. Rozenberg, Two-dimensional electron gas with universal subbands at the surface of SrTiO₃. *Nature* **469**, 189–193 (2011).
45. W. Meevasana, P. D. C. King, R. H. He, S.-K. Mo, M. Hashimoto, A. Tamai, P. Songsiriritthigul, F. Baumberger, Z.-X. Shen, Creation and control of a two-dimensional electron liquid at the bare SrTiO₃ surface. *Nat. Mater.* **10**, 114–118 (2011).
46. R. Bel, K. Behnia, H. Berger, Ambipolar Nernst effect in NbSe₂. *Phys. Rev. Lett.* **91**, 066602 (2003).
47. S. E. Rowley, L. J. Spalek, R. P. Smith, M. P. M. Dean, M. Itoh, J. F. Scott, G. G. Lonzarich, S. S. Saxena, Ferroelectric quantum criticality. *Nat. Phys.* **10**, 367–372 (2014).
48. J. J. Seo, B. Y. Kim, B. S. Kim, J. K. Jeong, J. M. Ok, J. S. Kim, J. D. Denlinger, S.-K. Mo, C. Kim, Y. K. Kim, Superconductivity below 20 K in heavily electron-doped surface layer of FeSe bulk crystal. *Nat. Commun.* **7**, 11116 (2016).
49. L. Rademaker, Y. Wang, T. Berlijn, S. Johnston, Enhanced superconductivity due to forward scattering in FeSe thin films on SrTiO₃ substrates. *New J. Phys.* **18**, 022001 (2016).
50. S. Coh, M. L. Cohen, S. G. Louie, Large electron-phonon interactions from FeSe phonons in a monolayer. *New J. Phys.* **17**, 073027 (2015).
51. Y. Wang, A. Linscheid, T. Berlijn, S. Johnston, Ab initio study of cross-interface electron-phonon couplings in FeSe thin films on SrTiO₃ and BaTiO₃. *Phys. Rev. B* **93**, 134513 (2016).
52. C. Bell, S. Harashima, Y. Kozuka, M. Kim, B. G. Kim, Y. Hikita, H. Y. Hwang, Dominant mobility modulation by the electric field effect at the LaAlO₃/SrTiO₃ interface. *Phys. Rev. Lett.* **103**, 226802 (2009).
53. H. M. Zhang, D. Zhang, X. W. Lu, C. Liu, G. Y. Zhou, X. C. Ma, L. L. Wang, P. Jiang, Q.-K. Xue, X. H. Bao, Origin of charge transfer and enhanced electron-phonon coupling in single unit-cell FeSe films on SrTiO₃. *Nat. Commun.* **8**, 214 (2017).
54. R. Loetzsch, A. Lubcke, I. Uschmann, E. Forster, V. Grosse, M. Thuerk, T. Koettig, F. Schmidl, P. Seidel, The cubic to tetragonal phase transition in SrTiO₃ single crystals near its surface under internal and external strains. *Appl. Phys. Lett.* **96**, 071901 (2010).
55. R. F. Egerton, *Electron Energy-Loss Spectroscopy in the Electron Microscope* (Springer Science & Business Media LLC, 2011).
56. Z. Li, J.-P. Peng, H.-M. Zhang, W.-H. Zhang, H. Ding, P. Deng, K. Chang, C.-L. Song, S.-H. Ji, L. L. Wang, K. He, X. Chen, Q.-K. Xue, X.-C. Ma, Molecular beam epitaxy growth and post-growth annealing of FeSe films on SrTiO₃: A scanning tunneling microscopy study. *J. Phys. Condens. Matter* **26**, 265002 (2014).

Acknowledgments: We thank J. Jain, D. H. Lee, K. F. Mak, B. Liu, X. Xi, L. Miao, and Q. Wang for fruitful discussions. **Funding:** This work was supported by the Penn State Materials Research Science and Engineering Centers (MRSEC), funded by the NSF under grant DMR-1420620. Work at Brookhaven National Library was supported by the U.S. Department of Energy, Office of Basic Energy Sciences, Division of Materials Science and Engineering, under contract no. DE-SC0012704. Work at Massachusetts Institute of Technology (MIT) was supported by grants from the NSF (DMR-1207469) and (DMR-0819762) (MIT MRSEC), the Office of Naval Research (N00014-13-1-0301), and the STC Center for Integrated Quantum Materials (under NSF grant DMR-1231319). W.Z. was supported by 1000 Plan for Young Talents of China and Open Research Fund Program of the State Key Laboratory of Low-Dimensional Quantum Physics (KF201701). **Author contributions:** W.Z., M.L., C.-Z.C., Y.Z., and M.H.W.C. designed the experiments. W.Z. made the devices and performed the transport measurements with the help of J.J. and M.H.W.C. C.-Z.C. grew the FeSe/STO films with the help of J.S.M. L.W. and M.L. performed the EELS measurements with the help of Y.Z. All authors participated in the analysis of the data and the preparation of the final manuscript. **Competing interests:** The authors declare that they have no competing interests. **Data and materials availability:** All data needed to evaluate the conclusions in the paper are present in the paper and/or the Supplementary Materials. Additional data related to this paper may be requested from the authors.

Submitted 1 July 2017

Accepted 7 February 2018

Published 16 March 2018

10.1126/sciadv.aao2682

Citation: W. Zhao, M. Li, C.-Z. Chang, J. Jiang, L. Wu, C. Liu, J. S. Moodera, Y. Zhu, M. H. W. Chan, Direct imaging of electron transfer and its influence on superconducting pairing at FeSe/SrTiO₃ interface. *Sci. Adv.* **4**, eaao2682 (2018).

Direct imaging of electron transfer and its influence on superconducting pairing at FeSe/SrTiO₃ interface

Weiwei Zhao, Mingda Li, Cui-Zu Chang, Jue Jiang, Lijun Wu, Chaoxing Liu, Jagadeesh S. Moodera, Yimei Zhu and Moses H. W. Chan

Sci Adv 4 (3), eaao2682.
DOI: 10.1126/sciadv.aao2682

ARTICLE TOOLS

<http://advances.sciencemag.org/content/4/3/eaao2682>

SUPPLEMENTARY MATERIALS

<http://advances.sciencemag.org/content/suppl/2018/03/12/4.3.eaao2682.DC1>

REFERENCES

This article cites 53 articles, 2 of which you can access for free
<http://advances.sciencemag.org/content/4/3/eaao2682#BIBL>

PERMISSIONS

<http://www.sciencemag.org/help/reprints-and-permissions>

Use of this article is subject to the [Terms of Service](#)

Science Advances (ISSN 2375-2548) is published by the American Association for the Advancement of Science, 1200 New York Avenue NW, Washington, DC 20005. The title *Science Advances* is a registered trademark of AAAS.

Copyright © 2018 The Authors, some rights reserved; exclusive licensee American Association for the Advancement of Science. No claim to original U.S. Government Works. Distributed under a Creative Commons Attribution NonCommercial License 4.0 (CC BY-NC).